

Modeling Urban Crime Occurrences via Network Regularized Regression

Elizabeth Upton¹ and Luis Carvalho²

1. Williams College, Department of Mathematics and Statistics
2. Boston University, Department of Mathematics and Statistics

Abstract

Analyses of occurrences of residential burglary in urban areas have shown that crime rates are not spatially homogeneous: rates vary across the network of city streets, resulting in some areas being far more susceptible to crime than others. The explanation for why a certain segment of the city experiences high crime may be different than why a neighboring area experiences high crime. Motivated by the importance of understanding spatial patterns such as these, we consider a statistical model of burglary defined on the street network of Boston, Massachusetts. Leveraging ideas from functional data analysis, our proposed solution consists of a generalized linear model with vertex-indexed covariates, allowing for an interpretation of the covariate effects at the street level. We employ a regularization procedure cast as a prior distribution on the regression coefficients under a Bayesian setup, so that the predicted responses vary smoothly according to the connectivity of the city. We introduce a novel variable selection procedure, examine computationally efficient methods for sampling from the posterior distribution of the model parameters, and demonstrate the flexibility of our proposed modeling structure. The resulting model and interpretations provide insight into the spatial network patterns and dynamics of residential burglary in Boston.

Keywords: graph Laplacian, network inference, residential burglary

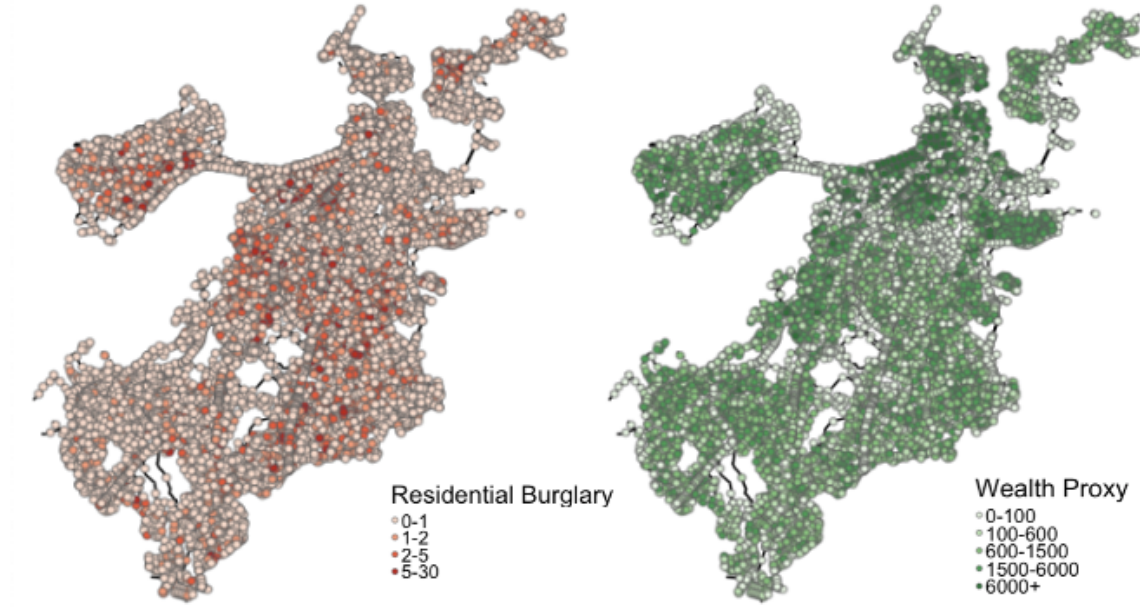


Figure 1: Residential burglary occurrence counts (left) and average wealth estimate in thousands of dollars (right) for street segments in the network of Boston, MA.

1 Introduction

While the modeling and forecasting of crime have been of interest to law enforcement and governmental agencies for some time, the recent availability of large crime datasets in urban areas has substantially increased and advanced these efforts. Here, we are interested in a specific type of crime, residential burglary, legally defined as “the act of breaking and entering a building with the intent to commit a felony” (Garner 2001). Using the GPS coordinates of reported burglaries (Open Data 2016), we mapped each crime occurrence (from June 2015 through December 2019) to its street segment. We then defined the dual network graph of Boston (Porta et al. 2006), where street segments are represented as nodes and edges are placed between any two which share an intersection. Figure 1 pictures the network, with each vertex color-coded to indicate our attribute of interest, counts of residential burglary.

A naive approach to modeling crime counts across the network would entail identifying a set of predictor attributes describing each street segment and performing count regression. For example, if Y_v and \mathbf{x}_v are the crime occurrence counts and covariate attributes at vertex v , we could suppose $Y_v \stackrel{\text{ind}}{\sim} \text{Po}[\exp(\mathbf{x}_v^T \beta)]$. However, this specification assumes that the effects β are constants across

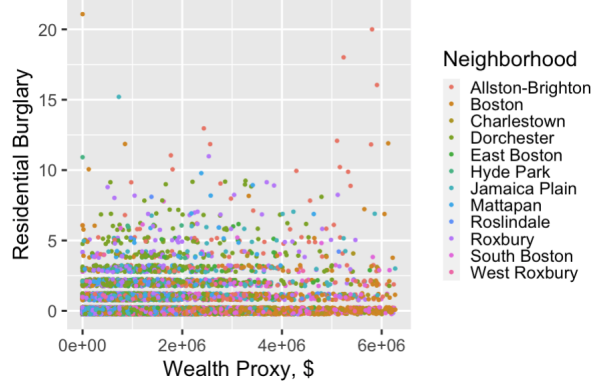


Figure 2: Counts of residential burglary (slightly jittered) versus wealth estimate by neighborhood for each street segment; illustrates the nonconstant effects of wealth on crime. To enhance the visualization, we exclude street segments with wealth estimates greater than the 95th percentile (\$6,272,010).

the network and empirical evidence suggests this is not the case. For example, Figure 1 displays gross tax information for the city of Boston in 2015. Comparing this attribute to the counts of residential burglary, we see that in some areas of the city lower taxes, identifying poorer communities, correspond to larger crime rates; however, in other locations, higher taxes indicative of wealth, correlate with higher crime rates. This is illustrated more clearly in Figure 2 where we see counts of residential burglary versus the wealth proxy by street segment; the correlation between these two variables is 0.15. Thus, even when including informative covariates, a regression with constant effects cannot adequately explain the variability in burglary occurrences across a city.

Additionally, the existence of crime “hot spots”, areas of concentrated crime counts, is widely acknowledged in crime theory literature (see, e.g., Eck et al. 2005). These zones can be identified visually in Figure 1; for example, in the southern region of the northwest peninsula neighborhoods, Allston and Brighton. Many current crime mapping algorithms focus on identifying these hot spots and estimate future crime risk based on past crimes (Bowers et al. 2004, Kim et al. 2018). However, interpretative models providing probabilities of hot spot formulation accounting for and explaining non-homogeneous effects are lacking.

A street network approach to crime modeling is beneficial, as it allows for the creation of a high-resolution spatial model. The measurements of distance utilized by the model are based on street length, connectivity, and walkability, naturally incorporating environmental and structural barriers

within the urban landscape. Furthermore, the connection between urban configurations and crime patterns aligns with key criminological theories. For example, crime pattern theory posits that criminals often target properties they encounter during non-criminal activities, linking the risk of a certain location being victimized to travel patterns that arise from every day activity (Davies & Johnson 2015). The hierarchical structure of city streets, with highly connected segments experiencing increased pedestrian and vehicle traffic, is captured in the network representation of the city and can be leveraged by a regression model that incorporates network information. Current approaches for modeling the spatial distribution of crime, such as point processes or areal/aggregate methods (Mohler et al. 2011, Balocchi & Jensen 2019) utilize Euclidean distance metrics, do not capture patterns at the street segment level, or focus primarily on forecasting as opposed to interpreting covariate effects.

Our proposed method aims to capture both gradual variations in crime explained by predictor attributes and abrupt variations attributed to hotspots. Most significantly, the model does not only identify areas of the city with extreme levels of residential burglary, but it identifies how factors contributing to these crimes change across the city. With this information, local law enforcement can direct crime prevention efforts to narrowly defined regions of the city and identify area specific interventions aimed at decreasing the occurrence rate of residential burglary.

1.1 Outline and Main Contributions

The outline of this paper is as follows: next, in Section 2, we introduce a regression model based only on the structure of a network. We then extend these ideas to include predictor attributes and cater our model to the needs of crime prediction. We also briefly discuss prior and related methodological work. In Sections 3 and 4, we provide guidelines for eliciting hyper-prior parameters and outline how to fit the model. In Section 5, we illustrate and compare the performance of our model on the Boston residential burglary data and simulated crime data. Finally, we conclude with a brief summary and discussion of future extensions in Section 6.

Our methodological contributions are outlined below, and details of each are discussed in the forthcoming text.

- We construct a *residential* street network of Boston by restricting the vertex set to street segments that abut residential parcels ($n = 12,763$). To maintain the connectivity of the entire vertex set on the reduced set, we utilize the Schur complement of the block of non-residential intersections on the full network Laplacian matrix.
- We address the issue of effect nonhomogeneity by vertex indexing our regression coefficients, allowing them to vary across the network. To accomplish this, we examine the eigendecomposition of the network Laplacian and adopt basis expansions of varying sizes composed of subsets of the eigenvectors of the Laplacian matrix for each coefficient.
- To avoid overfitting the model we impose smoothness on the linear predictor using a penalty based on a discrete differential operator induced by the network Laplacian matrix (Ramsay & Silverman 2005).
- To perform variable selection and determine the rank of each basis expansion we employ a novel sequential spike-and-slab prior on the basis expansion coefficients (George & McCulloch 1993). In the crime application, the rank of the basis expansion for each predictor variable allows an interpretation on the magnitude and variation of the predictor effect across the city.
- Addressing abrupt changes in crime rates, we use a latent network-indexed indicator to identify residential burglary hot spots. The indicator attribute assigns to each intersection its hot spot status, and is designed to vary smoothly over the network in the same manner as the other network predictors.
- The proposed hierarchical model is formalized in a Bayesian setup with Gaussian priors on the parameter sets. We use a block Gibbs sampler (Robert & Casella 2013) to draw samples from the posterior distribution of the model parameters. We also propose a computationally efficient expectation-maximization (EM) algorithm (Dempster et al. 1977) to find maximum *a posteriori* estimates of the parameters.

2 Proposed Model and Related Work

Our main methodological tool is *network regression*: given a network where vertices are connected by weighted edges, we observe vertex indexed data in the form of vertex attributes, and, as common in many applications, we distinguish between a response attribute of interest and a set of predictor attributes. To regularize the response attribute, we let the edge weights capture a measure of similarity between predictor attributes, as discussed shortly. Examples of representations of this data structure, beyond urban crime, include the infection status of individuals in a network of injection drug users given their drug use habits and other covariates such as age and gender; the political party affiliation of web blog authors in a network of hyperlinked connected blogs given the distribution of post topics and readership ideological inclinations; and the functional classes of proteins in a network of protein-protein interactions given gene pathway and other biological information (Leskovec & Krevl 2014).

We further abstract our problem of interest as follows: consider a weighted graph $G = (V, E, w)$ with vertex set V , edge set E , and positive weights w , that is, $w_{ij} > 0$ whenever $(i, j) \in E$ for all $i, j \in V$ and $w_{ij} = 0$ otherwise. We wish to regress a response Y on a set of predictor attributes X using a generalized linear model: for each vertex $v \in V$, $Y_v | \beta \stackrel{\text{ind}}{\sim} F[g^{-1}(\mathbf{x}_v^\top \beta(v))]$, where F belongs to an exponential family and g is a link function, and following our discussion, the network effects β are also vertex indexed.

2.1 Single-intercept model

Let us assume, for now, that we have a single-intercept model. Also, to directly apply the methodology to the crime application, we presume a count response: $Y_v | \beta \stackrel{\text{ind}}{\sim} \text{Po}[\exp(\beta(v))]$. To avoid overfitting, we impose smoothness on β through an informative prior that measures the roughness of β using a differential operator M_w and a roughness penalty $\lambda > 0$: $\beta \sim N(0, \lambda^{-1}(M_w^\top M_w)^-)$.

The maximum *a posteriori* (MAP) estimate $\hat{\beta}$ for β is then

$$\begin{aligned}\hat{\beta} &= \arg \max_{\beta} \left\{ \ell(\beta; Y) - \frac{\lambda}{2} \beta^\top M_w^\top M_w \beta \right\} \\ &= \arg \min_{\beta} \left\{ \mathcal{D}(Y, g^{-1}(\beta)) + \lambda \beta^\top M_w^\top M_w \beta \right\},\end{aligned}$$

where ℓ is the model log-likelihood and \mathcal{D} is the model deviance.

We take M_w to be the oriented weighted incidence matrix of the network: for $e = (i, j) \in E$, $M_{w,ei} = \sqrt{w_{ij}}$, $M_{w,ej} = -\sqrt{w_{ij}}$ and $M_{w,ev} = 0$ for all $v \in V$, $v \neq i$ and $v \neq j$. Thus $L_w = M_w^\top M_w = D_w - W$ is the weighted graph Laplacian with $W = [w_{ij}]$, the weighted adjacency matrix, and $D_w = \text{Diag}_{i \in V} \{ \sum_{j \in V} w_{ij} \}$, a diagonal matrix with the weighted degrees. In this sense, the prior on β is similar to an intrinsic conditional autoregressive model (ICAR; Besag et al., 1991), but with adjacency weights. Note that $L_w \mathbf{1}_{|V|} = 0$ and so L_w is rank deficient, requiring the use of the generalized inverse L_w^- when defining the prior. Our choice of M_w is deliberate and designed to exploit information found in the structure of the network to inform our model. In fact, expanding the log prior we have

$$\beta^\top M_w^\top M_w \beta = \beta^\top L_w \beta = \sum_{(i,j) \in E} w_{ij} (\beta(i) - \beta(j))^2,$$

that is, the term penalizes the weighted sum of squared differences for coefficients of adjacent vertices in the network (Kolaczyk 2009). Thus, as usual in Bayesian inference, we seek estimates of $\beta(v)$ that balance representativeness with respect to our observed data Y and X in the likelihood with smoothness with respect to the network topology in the prior.

The network effects β can be conveniently represented using a basis expansion with respect to the eigenvectors of the operator L_w , a common approach in functional data analysis (Ramsay & Silverman 2005). More specifically, since L_w is symmetric it realizes an eigen-decomposition $L_w = \Phi \Xi \Phi^\top$, and we can take τ eigenvectors to represent β as $\beta = \Phi_{1:\tau} \theta$, where $\Phi_{1:\tau}$ contains the first τ eigenvectors of L_w , ordered by the eigenvalues $\xi_1 < \dots < \xi_\tau$. Using this formulation, the log

prior becomes (up to a constant)

$$-\frac{\lambda}{2}\beta^\top L_w \beta = -\frac{\lambda}{2}\theta^\top \Phi_{1:\tau}^\top \Phi \Xi \Phi^\top \Phi_{1:\tau} \theta = -\frac{\lambda}{2}\theta^\top \text{Diag}_{i=1,\dots,\tau}\{\xi_i\}\theta,$$

or equivalently, $\theta \sim N(0, \lambda^{-1} \text{Diag}_{i=1,\dots,\tau}\{\xi_i^{-1}\})$. This results in the MAP

$$\hat{\theta} = \arg \min_{\theta} \left\{ \mathcal{D}(Y, g^{-1}(\Phi_{1:\tau}\theta)) + \lambda \theta^\top \text{Diag}_{i=1,\dots,\tau}\{\xi_i\}\theta \right\}. \quad (2.1)$$

In Section 3 we discuss guidelines for specifying basis rank τ and roughness penalty λ .

2.2 Extending the intercept model

We want our model to include vertex indexed covariate information leading to better predictive power and further understanding of the vertex attribute process. That is, given p predictors, we wish to regress on

$$\eta_v = g(\mathbb{E}[Y_v]) = \beta_0(v) + x_{1v}\beta_1(v) + \dots + x_{pv}\beta_p(v).$$

We perform the same basis expansion described in the intercept model on each coefficient, using the first τ_j eigenvectors of L , yielding

$$\eta_v = \sum_{j=0}^p x_{jv}\beta_j(v) = \sum_{j=0}^p x_{jv}\phi_{\tau_j}^\top \theta_j$$

that is, with $\beta_j(v) = \phi_{\tau_j}^\top \theta_j$ where ϕ_{τ_j} is the v -th row in $\Phi_{1:\tau_j}$ and we identify $x_{0v} = 1$ for the intercept. We now let

$$D_X = [\Phi_{1:\tau_0} \text{Diag}_{v \in V}\{x_{1v}\}\Phi_{1:\tau_1} \cdots \text{Diag}_{v \in V}\{x_{pv}\}\Phi_{1:\tau_p}]$$

and $\theta = [\theta_0 \ \theta_1 \ \cdots \ \theta_p]$, allowing us to write the linear predictor as $\eta = D_X \theta$. Here, D_X is composed of block columns, stacked horizontally, while θ is made up of the vertically stacked θ_j . We choose to smooth η over the network, resulting in predictions for the vertex attribute that vary smoothly over the topology of G . This more general specification results in the prior

$\theta \sim N(0, \lambda^{-1}(D_X^\top L_w D_X)^{-})$ for the basis expansion coefficients. Moreover, it extends the posterior estimate in (2.1) to accommodate the roughness penalty $\lambda \eta^\top L_w \eta = \lambda \theta^\top D_X^\top L_w D_X \theta$:

$$\hat{\theta} = \underset{\theta}{\operatorname{argmin}} \left\{ \mathcal{D}(Y, g^{-1}(D_X \theta)) + \lambda \theta^\top D_X^\top L_w D_X \theta \right\}. \quad (2.2)$$

2.3 Incorporating abrupt changes

We next add flexibility to the model, allowing it to detect abrupt changes in the vertex attribute over the topology of the graph, by introducing a network-indexed latent binary variable Z ,

$$Z_v | \gamma \stackrel{\text{ind}}{\sim} \text{Bern} \left[\text{logit}^{-1}(U_v^\top \gamma(v)) \right]. \quad (2.3)$$

Here, a set of predictor attributes U and network-smoothed effects γ determine the odds of v belonging to a normal or changed state. In the context of modeling residential burglary, this variable allows us to discriminate between two crime rates: if $Z_v = 0$ the vertex is considered to be in a crime hot zone described by $D_x(v)^\top \theta$. If $Z_v = 1$ the vertex lies in an area of the city with a “background” crime rate, $X(v)^\top \zeta$ where ζ is constant across the network. The latent effects γ assume a basis expansion in a similar manner as the main effects β : $\gamma_j(v) = \phi_{\tau v}^\top \omega_j$, and so the linear effects are $U_v^\top \gamma(v) = D_U(v)^\top \omega$, with D_U defined similarly to D_X . Together we have

$$\begin{aligned} Y_v | \zeta, \theta, Z_v &\stackrel{\text{ind}}{\sim} \text{Po} \left[\exp(Z_v X(v)^\top \zeta + (1 - Z_v)(D_X(v)^\top \theta)) \right] \\ Z_v | \omega &\stackrel{\text{ind}}{\sim} \text{Bern} \left[\text{logit}^{-1}(D_U(v)^\top \omega) \right] \\ \theta &\sim N \left(0, \lambda_\theta^{-1}(D_X^\top L_w D_X)^{-} \right) \\ \omega &\sim N \left(0, \lambda_\omega^{-1}(D_U^\top L_w D_U)^{-} \right). \end{aligned} \quad (2.4)$$

2.4 Prior and related work

The single-intercept model of Eq. (2.1) is akin to kernel based regression methods used to operate on discrete input spaces, such as graphs (e.g. Kolaczyk 2009, Section 8.4). The graph Laplacian is often used in the formation of kernels when the goal is to approximate data on a graph; see Smola

& Kondor (2003) for a number of examples of kernels defined via the Laplacian. Kernel methods employ a penalized regression strategy, as in Eq. (2.1), where the predictor variables are derived from the kernel (Kolaczyk & Csárdi 2014). Similarly, Belkin et al. (2004) consider the problem of labeling a partially labeled graph through regularization algorithms using a smoothing matrix, such as the Laplacian, and discuss theoretical guarantees for the generalization error of the presented regularization framework.

While these model formulations capture information in the network topology, they do not allow us to easily incorporate pertinent covariates. Kernel methods have been extended to include information from multiple kernel functions, each arising from a different data source (Lancriet et al. 2004). In this case, the problem is often redefined as determining an optimal set of weights used to merge the various kernel matrices (Kolaczyk 2009). However, these methods often lack interpretability and suffer from computational issues. Research has also been performed on variable selection for graph-structure covariates (Li & Li 2008). The proposed procedure involves a smoothness penalty on the coefficients derived from the Laplacian, however, in this particular application it is the predictor variables that represent the vertices in a graph, and the presence or absence of an edge identifies correlated features. The question of interest revolves around identifying grouping effects for predictors that are linked in the network. While the machinery employed is similar to that previously discussed, the question of interest is essentially different.

With the increased popularity and availability of network data, developing a framework for regression models specific to network indexed data has become a focus of recent research. Li et al. (2019) discuss network prediction models that incorporate network cohesion, the idea that linked nodes act similarly, and node covariates. They develop the theoretical properties of their estimator and demonstrate its advantage over regressions that ignore network information. Similarly to Li et al., our model focuses on interpretability and generalization; learning about the network and the vertex attribute of interest by examining the covariate values and introducing a flexible framework adaptable to a variety of GLM settings. However, our method differs in that the coefficients are designed to vary over the network, addressing the non-homogeneity of covariate effects, and allowing for an interpretation of how a covariate’s influence on the attribute process of interest changes across the network. Furthermore, our hierarchical structure allows for both smooth and abrupt changes in

the process rate. These are critical extensions in modeling residential burglary, as dynamic patterns may exist between the residential burglary occurrences and the predictor attributes that depend on the local structure of the city.

There is also a growing body of literature that utilizes network analysis to examine the relationship between road structure and residential burglary (Mahfoud et al. 2019, Davies & Johnson 2015, Frith et al. 2017). Much of this work utilizes descriptive statistics calculated from the network, such as betweenness or closeness, and incorporates these metrics into a model as predictor variables. The structure of the network beyond these statistics is not considered, however, the cumulative results provide evidence that street network properties are a significant predictor of burglary. This illustrates the potential of leveraging network connectivity to better understand patterns of residential burglary. Additionally, there are a number of machine learning algorithms and software programs being utilized to perform real time predictive analysis of crime in urban areas (Meijer & Wessels 2019). Our methodology is not intended to compete with these big data approaches, but it can provide valuable information regarding current criminological theories. To the best of our knowledge, ours is the first implementation of network regularized regression at the street-segment level for modeling occurrences of urban crime. Furthermore the construction of our residential network is a novel contribution to the emerging research area of crime modeling via network analysis.

3 Prior Elicitation

Fitting the proposed model to data requires eliciting hyper-prior parameters. In particular, we need to select three main sets of parameters:

Laplacian weights w . The weights defining the Laplacian L_w measure similarity between nodes. In our application, an urban street network, we have a natural measure of distance: the travel distance between the midpoints of two street segments. A network range parameter is introduced to calibrate the transformation from distance to similarity.

Basis ranks τ_{cj} and τ_{bj} . The cardinalities of the network basis expansions (differentiated between the count and Bernoulli levels) for each predictor control how long-range, global network effects in D_X and D_U are captured. They are elicited based on a modified model using spike-and-slab variable selection (George & McCulloch 1993).

Roughness penalties λ_ω and λ_θ . These prior precision scale parameters control the amount of regularization or smoothing of coefficients γ and β , respectively. They are elicited based on a criterion to minimize prediction error, along with a hyper-parameter controlling the variance between spike and slab when selecting the ranks.

3.1 Eliciting weights

A natural similarity measure between adjacent street segments is an inverse of street distance. We employ an exponential decay function (Banerjee et al. 2014) to define weights, $w_{ij} \propto \exp\{-d(i, j)/\psi\}$ where $d(i, j)$ is the travel distance between the midpoint of street segment i and the midpoint of street segment j and ψ is a range parameter. We set $\max\{w_{ij}\} = 1$ to avoid identifiability issues with the roughness penalties (see Section 5.2 for details).

3.2 Controlling basis rank expansions

Here we describe the rank selection at the count level of our model. The process at the Bernoulli level is analogous, and we drop the count-level subscript to ease notation. Now, we would like each τ_j to be large enough so that the combination of the τ_j Laplacian eigenvectors reflects characteristics of our attribute process while keeping the computational expense of the model in check (Ramsay & Silverman 2005). To this end, we modify the model by setting a hyper-prior on the basis ranks τ_j and performing Bayesian variable selection via a spike-and-slab prior (George & McCulloch 1993) on the basis expansion coefficients. We adopt a simpler model structure,

$$\begin{aligned} Y_v | \theta &\stackrel{\text{ind}}{\sim} \text{Po}\left(\exp(D_X(v)^\top \theta)\right) \\ \theta_j | \tau_j &\stackrel{\text{ind}}{\sim} N\left(0, \lambda^{-1} M_{\tau_j}^{1/2} (D_{X_j}^\top L_w D_{X_j})^{-1} M_{\tau_j}^{1/2}\right) \end{aligned} \tag{3.1}$$

where, with $K \leq |V|$ the maximum basis rank, I the indicator function, and $D_{X_j} = \text{Diag}\{X_j\}\Phi_{1:K}$, we have $M_{\tau_j} = \text{Diag}_{i=1,\dots,K}\{I(i > \tau_j)V_0 + I(i \leq \tau_j)\}$. Here, $0 < V_0 \ll 1$ is a small value, set to 0 in our application, distinguishing between the variance of the spike and slab components. Thus, (3.1) is the model induced when the first τ_j components of θ_j are assigned to the slab, and the remainder to the spike.

For the hyper-prior we set

$$\mathbb{P}(\tau_j) = \begin{cases} 1 - \alpha_0, & \tau_j = 0 \\ \alpha_0(1 - \alpha_1), & \tau_j = 1 \\ \alpha_0\alpha_1\rho^{\tau_j-1} / \sum_{k=2}^K \rho^{k-1}, & \tau_j = 2, \dots, K. \end{cases} \quad (3.2)$$

Hyper-parameters $\alpha_0 = \mathbb{P}(\tau_j > 0)$ and $\alpha_1 = \mathbb{P}(\tau_j > 1 \mid \tau_j > 0)$ control the prior probability of predictor X_j being selected and having a network basis expansion, respectively. Thus, parameters α_0 and α_1 can be elicited directly based on expert opinion of the odds of a predictor being included in the model and, if that is the case, of varying in the network. Since $\rho = \mathbb{P}(\tau_j = i) / \mathbb{P}(\tau_j = i - 1)$ for $i = 2, \dots, K$, this parameter controls, in effect, the cardinality of the expansion. To specify ρ , we recommend first finding a representative value for $\bar{\tau} = \mathbb{E}[\tau_j]$ and then, given α_0 and α_1 , solving for ρ ; see Appendix A.1 for details. A reasonable choice for $\bar{\tau}$ is the smallest value such that $\sum_{k=2}^{\bar{\tau}} \xi_k^{-1} / \sum_{k=2}^K \xi_k^{-1}$ is bounded by a large value close to 1, e.g. 0.9, similar to the usual variance explained or scree plot methods used to retain components in principal component analysis. Recall, the eigenvectors are ordered by the eigenvalues, where $\xi_1 < \dots < \xi_{\tau_j}$, and the structure of the network may be governed by a small percentage of eigenvectors (similar to how singular value decomposition can be used to obtain a smaller rank representation of a matrix).

To select the basis ranks, we employ an ECM algorithm (Meng & Rubin 1993) for model (3.1) where we cycle over each j -predictor to infer conditional posterior modes for θ_j with τ_j as a latent variable (Ročková & George 2014). Rather than explore all possible 2^K subsets of eigenvectors of the weighted Laplacian, as usual in a variable selection setting, we traverse the eigenvectors sequentially to determine τ_j . Focusing on the j -th predictor and conditional on all the other predictors, for the E-step we need, at the t -th iteration, $\nu_{ji}^{(t)} \doteq \mathbb{P}(\tau_j < i \mid Y, \theta_j^{(t)})$, $i = 1, \dots, K$. For the CM-step,

we set $\theta_j^{(t+1)}$ by Poisson regressing Y on D_{X_j} with prior precision $\lambda(T(\nu_j^{(t)}) \circ (D_{X_j}^\top L_w D_{X_j}))$ where $D_{X_j} = [\text{Diag}\{X_j\}\Phi_{1:K}]$, operator \circ is the Hadamard (element-wise) product,

$$T(\nu) = \left[1 - \nu_{\max\{i,k\}} + (\nu_{\max\{i,k\}} - \nu_{\min\{i,k\}}) V_0^{-\frac{1}{2}} + \nu_{\min\{i,k\}} V_0^{-1} \right]_{i,k=1,\dots,K},$$

and an offset composed of the information from the remaining predictors in the model. After convergence, we select τ_j via *sequential centroid estimation*, which tends to be more robust than the usual conditional posterior mode and, in effect, picks the minimum number of eigenvectors such that the cumulative posterior is less than some threshold. This procedure is repeated for each one of the predictors in turn, continuously updating prior precisions and offsets, until τ does not change between consecutive cycles. See Appendices A.2 and A.3 for detailed presentations of the ECM algorithm and the sequential centroid estimator.

3.3 Selecting λ_θ , λ_ω

We use a leave-one-out cross validation PRESS statistic defined on the working responses in the final step of the iterative reweighted least squares (IRLS) algorithm, the usual computational routine used to fit generalized linear models (McCullagh & Nelder 1989). We call this the LOOP (leave-one-out-proxy) statistic,

$$\text{LOOP} = \sum_{v \in V} \frac{(Y_v - \hat{\mu}_{(v),v})^2}{V(\hat{\mu}_{(v),v})} \approx \sum_{v \in V} \frac{r_v^2}{1 - h_v},$$

where $\hat{\mu}_{(v),v}$ is the mean at v fitted without the v -th observation, $V(\mu)$ is the variance function ($V(\mu) = \mu$ for the Poisson model), $r_v = (Y_v - \hat{\mu}_v) / \sqrt{V(\hat{\mu}_v)}$ is the v -th Pearson residual, and h_v is the leverage at v .

We define D_X and D_U using the ranks found by the procedure in Section 3.2 and then minimize the LOOP statistic to determine λ_θ and λ_ω respectively. This process can be viewed as an empirical Bayes procedure where we maximize prediction accuracy rather than posterior density.

4 Model Inference

To estimate the model parameters, we sample from the joint posterior $\mathbb{P}(Z, \theta, \omega, \zeta | Y)$ using Gibbs sampling. We iterate sampling from the conditional distributions

$$[Z | \omega, \zeta, \theta, Y], \quad [\zeta | Z, \omega, \theta, Y], \quad [\theta | Z, \omega, \zeta, Y], \quad [\omega | Z, \omega, \zeta, Y], \quad (4.1)$$

until assessed convergence. Sampling Z is straightforward; we have

$$\mathbb{P}(Z | \omega, \zeta, \theta, Y) \propto \mathbb{P}(Y | \zeta, \theta, Z) \mathbb{P}(Z | \omega) = \prod_v \mathbb{P}(Y_v | \zeta, \theta, Z_v) \mathbb{P}(Z_v | \omega)$$

and so, referencing (2.4), we have $Z_v | \omega, \zeta, \theta, Y_v \stackrel{\text{ind}}{\sim} \text{Bern}(\gamma_v(\omega, \zeta, \theta))$ with

$$\text{logit} \gamma_v(\omega, \zeta, \theta) \doteq D_U(v)^\top \omega + Y_v X(v) \zeta - \exp(X(v) \zeta) - (Y_v D_X(v)^\top \theta - \exp(D_X(v)^\top \theta)). \quad (4.2)$$

To sample ζ , θ , and ω we first note that the likelihood in (2.4) can be rewritten to partition the data Y according to the latent indicators as

$$Y_v | Z_v = 1, \zeta \stackrel{\text{ind}}{\sim} \text{Po}(\exp(X(v)^\top \zeta)) \quad \text{and} \quad Y_v | Z_v = 0, \theta \stackrel{\text{ind}}{\sim} \text{Po}(\exp(D_X(v)^\top \theta)).$$

Sampling in the three last conditional steps in (4.1) is then equivalent to sampling coefficients from the posterior of a Poisson log-linear model, in the case of ζ and θ , and a logistic model, in the case of ω , with normal priors as stated in (2.4). Each conditional step is a Metropolis-within-Gibbs step, using a one-step Riemannian manifold Hamiltonian Monte Carlo proposal, also known as a manifold Metropolis adjusted Langevin algorithm (MMALA; see Girolami & Calderhead 2011). We describe this process and outline the proposal density and acceptance probability in Appendix B.2.

Due to the potentially large scale of data in common applications, the above sampling scheme may be slow to converge. We thus suggest finding initial values for the sampler via an EM algorithm with Z as a latent variable; see details in B.1. For the E-step we compute, at the t -th iteration, $\pi_v^{(t)} = \mathbb{E}[Z_v | \omega^{(t)}, \zeta^{(t)}, \theta^{(t)}, Y_v] = \gamma_v(\omega^{(t)}, \zeta^{(t)}, \theta^{(t)})$, with γ_v as in (4.2). The three M-steps are then

as follows:

M-step for ζ : set $\zeta^{(t+1)}$ by quasi-Poisson regressing $\pi^{(t)}Y \sim X$ with offset $\log \pi^{(t)}$;

M-step for θ : set $\theta^{(t+1)}$ by quasi-Poisson regressing $(1 - \pi^{(t)})Y \sim D_X$ with offset $\log(1 - \pi^{(t)})$ and $\lambda_\theta D_X^\top L_{w(\psi)} D_X$ as prior precision;

M-step for ω : set $\omega^{(t+1)}$ by quasi-binomial regressing $\pi^{(t)} \sim D_U$ with $\lambda_\omega D_U^\top L_{w(\psi)} D_U$ as prior precision.

5 Data Analysis and Results

We now turn to our application and conduct two studies around residential burglary occurrences in Boston, MA: a simulation study and a more detailed case study. The data, provided by the city of Boston and available to the public (City of Boston 2016, Open Data 2016) contain information on the 5,741 instances of residential burglary occurring between June 2015 and December 2019 in central Boston. The covariate data, as described below, was constructed from a variety of publicly available shape files. The code used to perform the analyses, with links to shape files, is available in the supplementary materials.

The first step in applying our modeling procedure is to clearly define our network of interest. A city can be intuitively represented as a network by designating street intersections as nodes and street segments as edges, as visualized for a small area of Boston in the left panel of Figure 3 (this is often referred to as the primal representation). However, given that residential burglary predominantly occurs along street segments rather than at intersections, utilizing street segments as the main unit of analysis, i.e. the vertices, yields a more representative network. Moreover, given that the exact location of each crime is sensitive, recording it in aggregated form by street segment guarantees some level of confidentiality. This formation is pictured in the right panel of Figure 3 and is often referred to as the dual representation (Porta et al. 2006). In graph theory, the dual network is also known as the line graph of the primal network. We note that while the edges are visualized as straight lines, the weight of each edge is the street distance from the midpoints

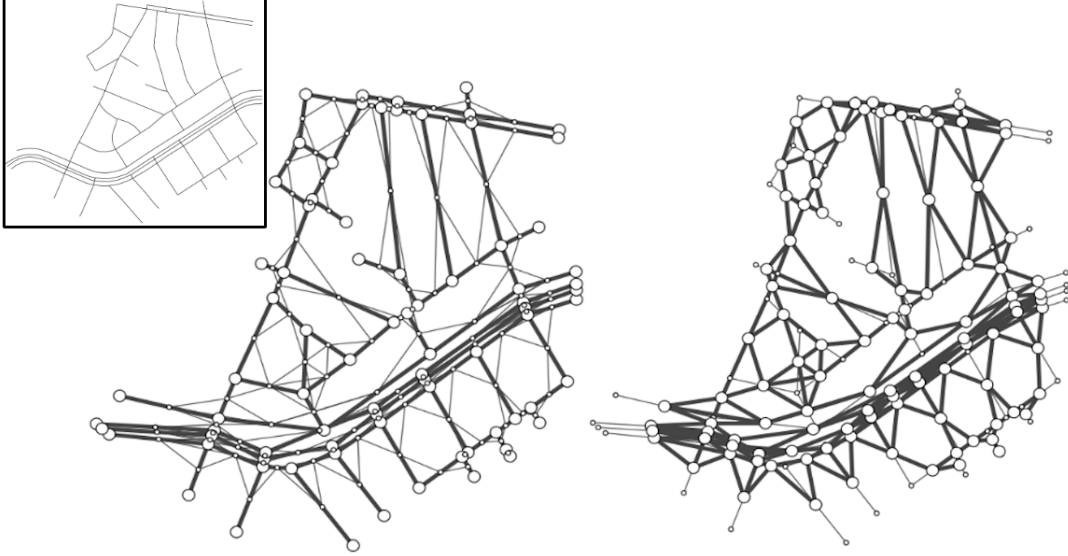


Figure 3: Comparison of primal (left) and dual (right) network representations. To ease comparison, each network is superimposed on the other (thin edges and small nodes). The black box in the upper left is the map visualization of the area.

of the street segments (not the Euclidean distances). This better captures the connectivity of the city through the perspective of a potential criminal.

Although we have covariate and response data for each street segment in the city of Boston, only those segments in residential areas can experience the response of interest, occurrences of residential burglary. Thus, we want to restrict the vertex set to street segments that abut residential parcels while not losing the connectivity information in the entire street network. We accomplish this through the Kron reduction process (Dorfler & Bullo 2012), which maintains effective resistances (graph-theoretic distances between nodes) while reducing the node set. Specifically, given a set of v vertices to be marginalized out in a weighted graph, we need to compute the Laplacian of $G[-v]$ in order to fit our model. Partitioning the street segments in our network into residential, R , and non-residential, N , segments, we can similarly partition the weighted Laplacian L of G into blocks L_{RR} , $L_{RN} = L_{NR}^\top$, and L_{NN} . We then find the weighted Laplacian of $G[-N]$ to be $L_{RR} - L_{RN}L_{NN}^{-1}L_{NR}$, the Schur complement of N in L . Our resulting *residential* network of Boston is composed of 12,763 street segments (as compared to 15,078). Figure 4 illustrates the process on a small section of Boston, where the left image displays the residential parcels in the city, and the right displays the street map. Street segments highlighted in yellow remain in the vertex set,

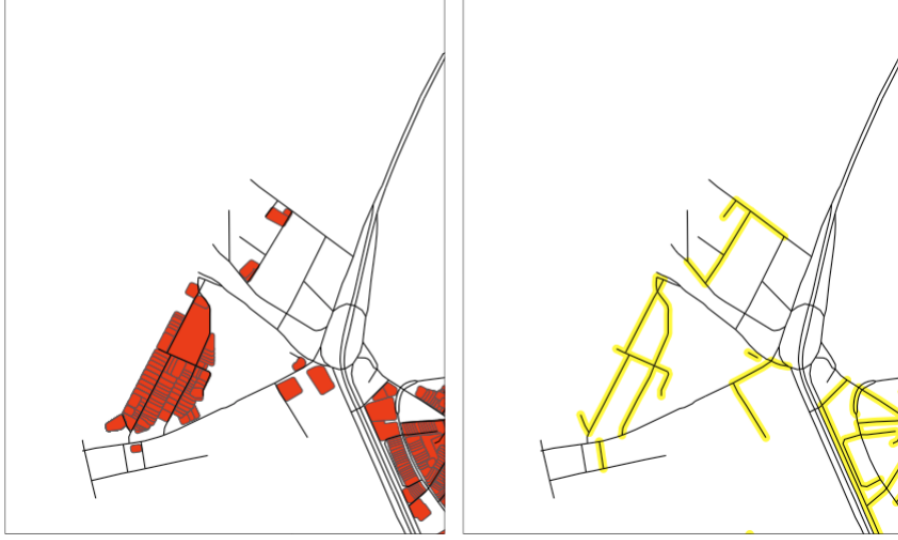


Figure 4: Illustration of residential parcels in red (left) and street segments remaining in the vertex set in yellow (right) on a small region in Boston, MA.

but those in gray are marginalized out. As expected, all street segments marginalized out from the network saw zero occurrences of residential burglary in the time frame of the data.

The street segment attributes gathered and included in our final model are:

Population: population size, based on census tracts from the US Census Bureau, 2010

Gross tax: property tax surrounding each street segment. To calculate, we construct a buffer around each street segment, capturing the residential partials abutting the street, and then sum the gross tax from each parcel. The results are visualized in Figure 1.

Distance to nearest police station: street distance from the center of each segment to the nearest police station.

University/college housing indicator: binary indicator set equal to one if college/university housing is located on the street segment.

The population effect is assumed constant across the network, that is, we consider it as an exposure variable, while the other covariate effects are subject to the results of the basis rank selection. Our choice of analyzing the aforementioned covariates was driven by established crime

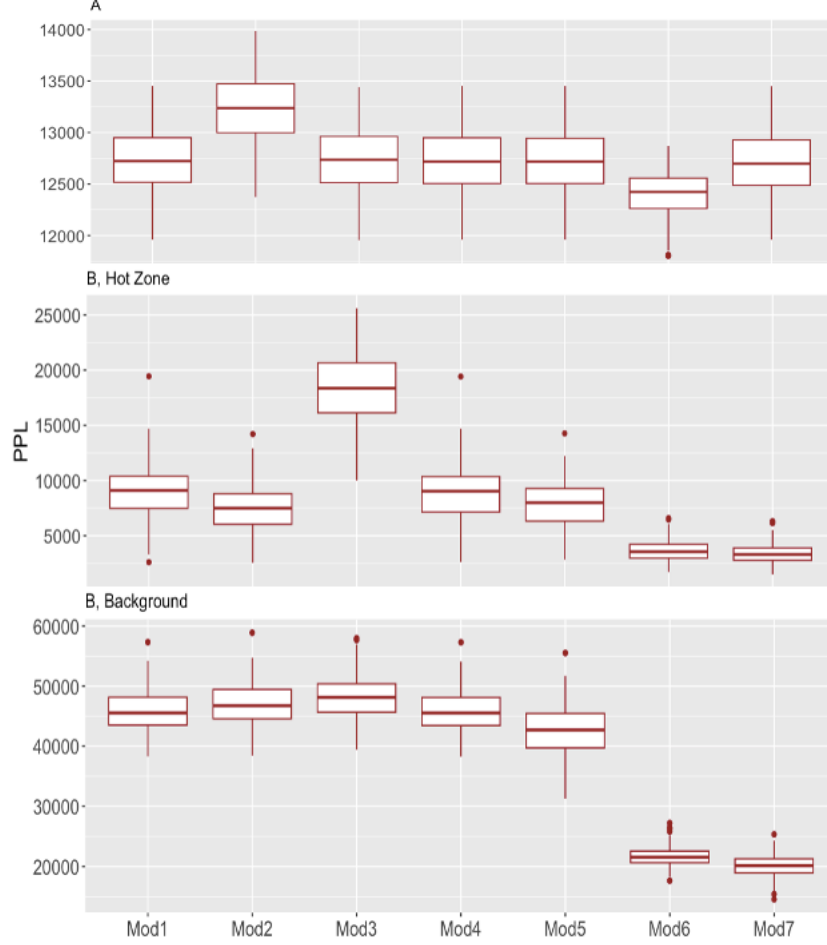


Figure 5: We compare posterior predictive loss (PPL) for two simulations. A: Simple data generating process, B: Complex data generating process. For simulation B, we present PPL for street segments in and out of hot zones according to the simulation scheme.

theory (Bernasco & Block 2009) and publicly available data. The model could easily be extended to include additional covariates of interest.

5.1 Simulation study

In order to assess the performance of our model (**Mod7**, in (2.4)) we compare its output in two different simulation studies against six competing methods:

Mod1: Intercept-only Poisson regression, akin to Laplacian kernel regression, $Y_v | \theta \stackrel{\text{ind}}{\sim} \text{Po}[\exp(\phi_{\tau v}^\top \theta)]$ and $\theta \sim N(0, \lambda^{-1} \text{Diag}_{i=1, \dots, \tau} \{\xi_i\}^-)$.

Mod2: Intercept-only Poisson regression, akin to kernel regression, utilizing the diffusion kernel of Smola & Kondor (2003).

Mod3: Poisson regression using the covariates, but ignoring the network similarity, $Y_v | \theta \stackrel{\text{ind}}{\sim} \text{Po}[\exp(\mathbf{x}_v^\top \beta)]$.

Mod4: A Poisson network cohesion model in the flavor of that proposed by Li et al. (2019). In essence, we assume a basis expansion of the intercept only and set all other basis ranks, τ_j , to one.

Mod5: Poisson regression defining D_X and smoothing the linear predictor, but ignoring the abrupt changes in the network, $Y_v | \theta \stackrel{\text{ind}}{\sim} \text{Po}[\exp(D_X(v)^\top \theta)]$ and $\theta \sim N(0, \lambda^{-1}(D_X^\top L_w D_X)^-)$.

Mod6: Intercept-only Poisson regression, akin to kernel regression, that takes into account abrupt changes in the network $Y_v | \zeta, \theta, Z_v \stackrel{\text{ind}}{\sim} \text{Po}[\exp(Z_v \zeta + (1 - Z_v) \phi_{\tau_v}^\top \theta)]$, $Z_v | \omega \stackrel{\text{ind}}{\sim} \text{Bern}[\text{logit}^{-1}(\phi_{\tau_v}^\top \omega)]$, $\theta \sim N(0, \lambda^{-1} \text{Diag}_{i=1, \dots, \tau} \{\xi_i\}^-)$ and $\omega \sim N(0, \lambda^{-1} \text{Diag}_{i=1, \dots, \tau} \{\xi_i\}^-)$.

For the simulations, we use the residential street network ($n = 1,278$) information for Allston/Brighton (the northwest peninsula neighborhoods of Boston, pictured in Figure 11 in the appendix). This part of the city is not included in our case study (see discussion below), however, we make use of the available covariate and network structure for two simulations:

- A: We generate random crime counts on each street segment from a Poisson distribution with constant mean.
- B: We generate random crime counts on each intersection using the negative-binomial distribution with mean $\mu = \exp(Z_v \zeta + (1 - Z_v)(D_X(v)^\top \theta))$ and variance $\mu + \mu^2$. We chose to sample from the negative-binomial distribution given that crime data are often over-dispersed. For Z_v , we designate three hot zones, using the breadth-first search algorithm originating at three randomly chosen intersections and capturing 10% of the nodes (Cormen et al. 2001). To construct D_X we set a universal τ_j , and sample θ from the prior distribution given in (2.4). Lastly, we set ζ , a background crime rate, equal to -2.5 which was found to create a range of crime counts similar to that of the observed data.

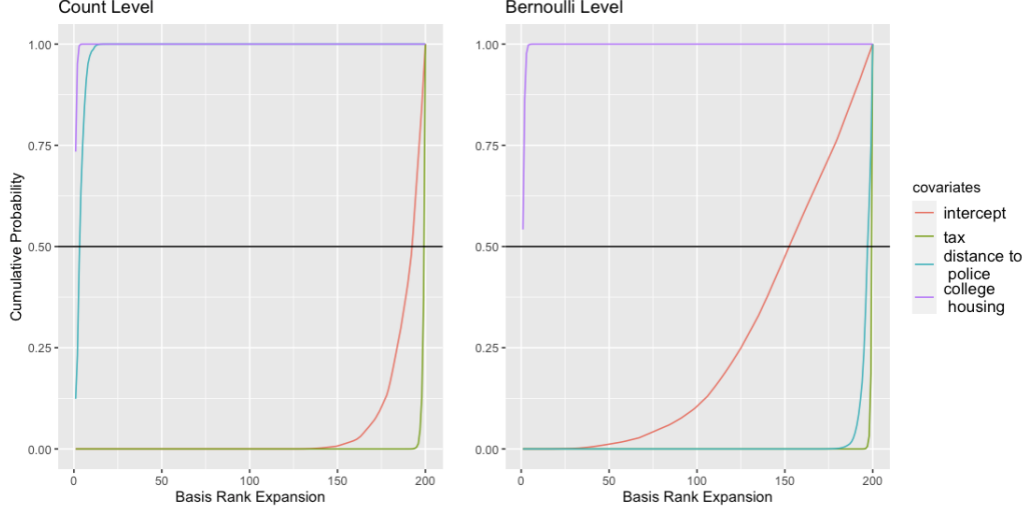


Figure 6: Choosing τ , the rank of the coefficient effects, based on a threshold of 0.5.

We complete the seven regressions of interest and compare their performance based on posterior predictive loss, a proxy for out of sample prediction. For this exercise, we forgo our Gibbs sampling algorithm and use the posterior modes calculated through the EM-algorithm as coefficient estimates. For **Mod1**, **Mod2**, **Mod4** and **Mod5**, we choose τ based on the LOOP. For **Mod6** and **Mod7** we define τ_j and λ using the procedure described in Section 3.2.

As shown in Figure 5, **Mod7** does not degrade in performance due to increased model complexity. That is, the model has protection against overparameterization due to the rank selection process. In 139 out of the 200 simulations, the τ_j value for each of the j predictors was 1, indicating the process determined that a basis expansion was not informative.

Mod7 outperforms the competing methods for intersections in and out of the three hot zones. Furthermore, **Mod5** shows improvement over **Mod4**, indicating that **Mod5** (and **Mod7**) explains additional variation in crime counts by allowing the coefficient effects to vary smoothly over the network. **Mod6** and **Mod7** illustrate the effectiveness of the hotzone indicator to differentiate between the two different crime rates.

5.2 Case study: Boston, Massachusetts

We now analyze the entire metropolitan region of Boston, excluding Allston/Brighton and East Boston (see Figure 11). These parts of Boston are separated from Boston proper: East Boston can only be accessed via ferry boat or tunnel and Allston’s southern border town (Brookline) is not part of Boston. Because we don’t have access to network and crime reporting data for Brookline, the network depiction of the city suggests a disconnection of Allston from Boston that is misleading. Numerous pathways traverse Brookline, linking Allston to Boston, and the absence of this information results in an inaccurate representation of Allston’s connectivity with the broader city. That being said, one could perform the analysis separately on these two neighborhoods.

Following the guidelines in Section 3, the network range parameter, ϕ , is set to 0.15, resulting in a median similarity weight of 0.8 in the adjacency matrix. All continuous predictor variables were log-transformed and scaled. The background crime rate, described by $X(v)^\top \zeta$ in (2.4), is based only on population. The maximum basis expansion rank was set to 200 (based on exploratory analysis), and, following Section 3, $\alpha_0 \doteq 1, \alpha_1 \doteq 0.99$ and $\sum_{k=2}^{\bar{\tau}} \xi_k^{-1} / \sum_{k=2}^K \xi_k^{-1}$ is bounded by 0.9 in order to determine $\bar{\tau} = 68$. These hyperparameters were chosen to give relatively high probabilities of variable inclusion and expansion. For the ECM algorithm in Section 3.2, V_o is set to zero, and Figure 6 displays the cumulative posterior results, $\mathbb{P}(\tau_j | Y, \theta_j)$ for each predictor at both the count and Bernoulli levels of the model. We included the same set of predictor variables in both levels of the model, but this is not required.

As posited in the introduction, the gross tax effect varies over the network and is best captured via a basis expansion of large rank; conversely, distance to the nearest police station requires a smaller basis expansion at the Count level of the model and the effect of college housing appears to be constant across the network. The connection between the covariate and its rank gives some indication of the complexity of the variable’s relationship to the process rate being modeled. For example, given that most college housing occurs in two small areas of Boston proper, it makes sense that the effect of this indicator variable on residential burglary counts does not vary across the city. Given the basis expansion ranks, we construct D_X and D_U and, using the LOOP, determine λ_θ and λ_ω . The MAP estimates found using the EM algorithm are used as initial values in the Gibbs

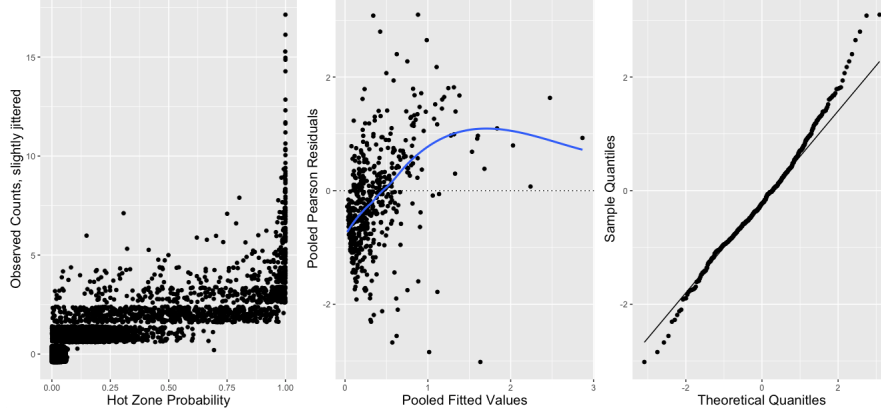


Figure 7: Observed counts versus latent values, $1 - \pi_i$ (left), Pooled Pearson residuals versus fitted values (middle) and normal quantile comparison plot (right).

sampler. Figure 10, included in the appendix, displays the posterior distributions of a selection of statistics, and are based on 1000 samples, after discarding 20% for a burn-in period and thinning every 10. We ran multiple chains and assessed convergence of the Gibbs sampler by analyzing trace plots and evaluating rank-based \hat{R} and effective sample size (ESS; Vehtari et al. 2019). Of note, the EM algorithm provides reasonable point estimates and is computationally efficient (we include supporting evidence of this in Appendix B.3).

Diagnostic plots from the fitted model are in Figure 7. We see that the hot zone probabilities align well with the observed counts of residential burglary. The plot of the binned Pearson residuals (response residuals divided by the non-constant variance estimate, as typically utilized when assessing a GLM) versus the fitted values is relatively null given our dependent variable is discrete. Furthermore, the normal quantile plot of the Pearson residuals does not suggest a strong departure from normality; while crime data is often over-dispersed or zero-inflated, the creation of our *residential* network and the hot zone indicator addresses these issues. However, the outlined methodology, including the EM algorithms, is easily adapted to other exponential random family distributions. For example, we explored utilizing the negative-binomial distribution and found that the additional precision parameter in the distribution introduces too much flexibility. That is, using the Poisson distribution, the distribution of hot zone probabilities is bi-modal, with peaks near 0 and 1. Using the negative-binomial distribution resulted in the distribution having greater mass towards 0.5, creating “luke warm” zones. This decreased the predicted crime rates for intersections

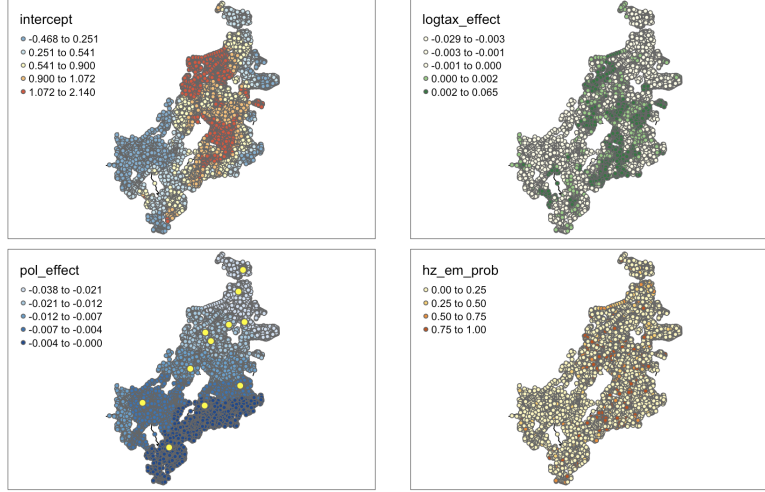


Figure 8: Covariate effects across the city for the count level of the model. Yellow bubbles on police effect (bottom left) indicate the location of police departments. The bottom right plot shows the latent values, $1 - \pi_i$ describing the probability of each intersection being in an hot zone.

located in hot zones and underestimated the occurrences of residential burglary.

The interpretational power of our model is of primary interest. Figure 8 summarizes the effects, $\beta(v) = \phi_\tau^T \theta$, of the intercept, wealth/tax, and distance to nearest police station. While the exact values for each street segment are not displayed, the gradation scales allow us to identify areas of the city where the effects of each covariate are most pronounced (in this case, the coefficients have the same interpretation as in a Poisson regression). Individual estimates and significance levels per street segment could be evaluated by referencing the posterior distributions.

On the tax effect plot, notice the large number of dark green intersections down the central corridor of the city (originating in the Fenway/South End neighborhood down through Mattapan and South Dorchester), identifying areas where the tax effect on residential burglary is greatest. It is noteworthy that this corridor was recently identified as socially vulnerable (Cleveland et al. 2019) and highly susceptible to gentrification and displacement (City of Boston 2022). Boston’s published displacement indices are calculated based on 16 indicators encompassing demographic factors (e.g. race, housing cost burden, educational attainment), amenities (e.g. access to public transportation) and market changes (e.g. rent appreciation, commercial development). While the connection between urban displacement and crime levels is an area of active research with some evidence supporting gentrification reducing crime (Palmer et al. 2017), it could also be that these

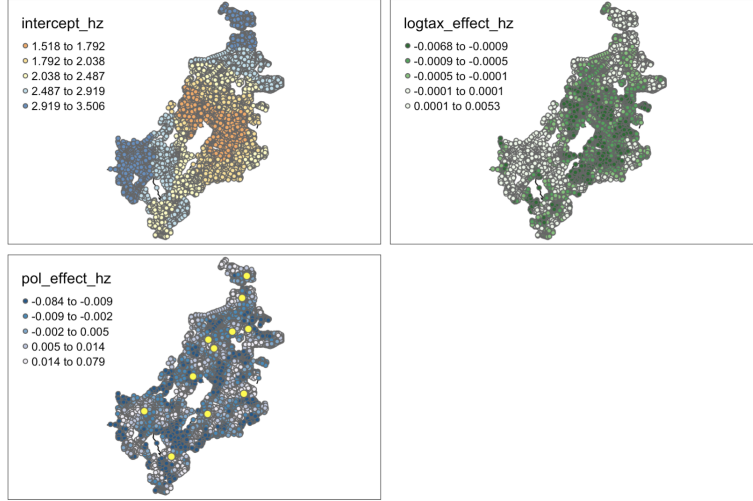


Figure 9: Covariate effects across the city for the hot zone indicator level of the model. Recall, if $Z_v = 0$ the vertex is considered to be in a crime hot zone, so negative effects contribute to a larger probability of a street segment being designated as in a hot zone.

neighborhood dynamics result in target rich environments for residential burglary. More specifically, residential parcels with higher property taxes may be particularly susceptible to occurrences of residential burglary in this area of the city.

Notably, the police effect at the count level of the model is quite smooth across the city given its small basis rank expansion. However, Figure 9, illustrating the effects at the hot zone indicator level, tells a more nuanced story. Here we see darker street segments (identifying the larger covariate effects) between the southern neighborhoods of the city (Mattapan, Hyde Park, and Roslindale). There also exists strong effects on the northern border of the open space, Franklin Park, in the center of the city (Roxbury). This identifies areas of Boston where a lack of police presence may be contributing more greatly to the observed crime than in other areas. Looking at Figures 8 and 9 collectively gives evidence that proximity to police contributes more to the hot zone status of a street segment and, given that status, the wealth effect is more informative at the Count level.

Additional predictors could be included in the outset of the model formulation to identify their effects across the city. This information is beneficial to residents of Boston, local law enforcement agencies seeking to optimize their resources, and urban planners responding to the city's evolving needs.

6 Conclusions

We have presented a method of Bayesian network regularized regression for modeling vertex attributes that incorporates both relevant covariates and topological information in its construction. The resulting model is composed of node indexed coefficients, regularized using the Laplacian matrix, producing fitted values that vary smoothly over the network. This machinery, including the corresponding variable selection techniques and EM algorithms, is widely applicable and easily adaptable to a variety of GLM settings. As previously mentioned, in general, we could regress a response attribute Y on network-indexed coefficients, $Y_v | \beta \stackrel{\text{ind}}{\sim} F[g^{-1}(\mathbf{x}_v^\top \beta(v))]$, where F belongs to the exponential family and g is a link. Furthermore, the described methods can be modified to include specific characteristics of the network being analyzed (e.g. hot spots); the flexibility of the introduced contributions is valuable.

Our network approach to modeling occurrences of residential burglary allows us to incorporate environmental and structural barriers in the connectivity of the city. The similarity calculations are based on a metric of walkability and naturally lend themselves to describing possible patterns in residential burglary. Perhaps most significantly, the model results provide a clear picture of how factors contributing to the response variable vary across the network. This is particularly useful when applied to modeling residential burglary: crime rates are not homogeneous, and understanding why specific regions or street segments experience high crime is valuable information.

Our analysis has prompted a variety of additional research inquiries that could extend the current work. For example, while we have chosen to focus on modeling the spatial variation in residential burglary, many crime prediction algorithms are concerned with temporal variations or the interplay between time and space. A relatively straightforward way to extend the current methodology would be to fit distinct models to consecutive time frames of interest and analyze variations in the coefficient estimates over time. This mirrors approaches aimed at quantifying the efficacy of crime intervention initiatives, where model outcomes predicting the probability of a crime are compared using data from before and after the intervention occurs (Johnson et al. 2014). A more ambitious approach could be to develop a Bayesian dynamic model that allows the coefficients to evolve over both time and space, and for the probability distributions to be updated

as new data becomes available.

A Prior Elicitation

A.1 Selecting ρ

Given hyper-prior parameters α_0 and α_1 and mean basis rank $\bar{\tau}$, we need to solve, according to the prior on τ_j in (3.2),

$$\begin{aligned}\mathbb{E}[\tau_j] &= \alpha_0(1 - \alpha_1) + \alpha_0\alpha_1 \frac{\sum_{k=2}^K k\rho^{k-1}}{\sum_{k=2}^K \rho^{k-1}} \\ &= \alpha_0(1 - \alpha_1) + \alpha_0\alpha_1 \left(1 + \frac{\sum_{k=1}^{K-1} k\rho^k}{\sum_{k=1}^{K-1} \rho^k}\right) = \bar{\tau}.\end{aligned}$$

Let $S(\rho) \doteq \sum_{k=1}^{K-1} k\rho^k$. Then $(1 - \rho)S(\rho) = \sum_{k=1}^{K-1} \rho^k - (K - 1)\rho^K$ and $\sum_{k=1}^{K-1} \rho^k = \rho(1 - \rho^{K-1})/(1 - \rho)$, thus,

$$\frac{\bar{\tau} - \alpha_0}{\alpha_0\alpha_1} = \frac{S(\rho)}{\sum_{k=1}^{K-1} \rho^k} = \frac{1}{1 - \rho} - \frac{(K - 1)\rho^{K-1}}{1 - \rho^{K-1}}.$$

The solution, constrained to $\rho > 0$, can be solved numerically using standard procedures such as Newton's method.

A.2 Selecting τ_j

To select τ_j (we drop the subscript j for the remainder of this discussion), the rank of the basis expansion for each covariate in the model, we adopt a *sequential centroid estimator*. Let us first define an auxiliary variable $\omega(\tau)$ that represents τ as an indicator vector: $\omega(\tau)_i = I(i \leq \tau)$, for $i = 1, \dots, K$. For instance, $\omega(0) = (0, 0, \dots, 0)$, $\omega(1) = (1, 0, \dots, 0)$, and so on, with $\omega(K) = \mathbf{1}_K$. Note the one-to-one correspondence between τ and ω , and thus, while $\tau \in \mathcal{T} \doteq \{0, \dots, K\}$, ω only takes values in $\Omega \doteq \cup_{j \in \mathcal{T}} \omega(j)$.

Now, given the marginal posteriors $\mathbb{P}(\tau | Y)$ or the EM-conditional posteriors $\mathbb{P}(\tau | Y, \theta^{(t)})$, which we denote in general by π_τ , we define a Bayes estimator $\hat{\tau}$ according to a generalized Hamming

gain G on the ω -map:

$$\hat{\tau} \doteq \arg \max_{\tilde{\tau} \in \mathcal{T}} \sum_{\tau \in \mathcal{T}} G(\omega(\tilde{\tau}), \omega(\tau)) \pi_{\tau}.$$

When comparing two indicator ranks, the gain function G assigns zero gain to each discrepancy between them, a unit gain to matched zeroes (true negatives) and a gain of $\kappa > 0$ to matched ones (true positives). For example, if $K = 7$, then $G(\omega(3), \omega(5)) = 2 + 3\kappa$ since there are three matched ones from positions 1 through 3, two mismatches from positions 4 and 5, and two matched zeros from the last two positions, 6 and 7. Thus,

$$G(\omega(\tau_1), \omega(\tau_2)) = K - \max\{\tau_1, \tau_2\} + \kappa \min\{\tau_1, \tau_2\}.$$

Then,

$$\begin{aligned} \hat{\tau} &= \arg \max_{\tilde{\tau} \in \mathcal{T}} \sum_{\tau \in \mathcal{T}} \left(\kappa \min\{\tau, \tilde{\tau}\} - \max\{\tau, \tilde{\tau}\} \right) \pi_{\tau} \\ &= \arg \max_{\tilde{\tau} \in \mathcal{T}} \left\{ \sum_{\tau \leq \tilde{\tau}} (\kappa \tau - \tilde{\tau}) \pi_{\tau} + \sum_{\tau > \tilde{\tau}} (\kappa \tilde{\tau} - \tau) \pi_{\tau} \right\} \\ &= \arg \max_{\tilde{\tau} \in \mathcal{T}} \left\{ \sum_{\tau \leq \tilde{\tau}} ((\kappa + 1)\tau - \tilde{\tau}) \pi_{\tau} + \sum_{\tau > \tilde{\tau}} \kappa \tilde{\tau} \pi_{\tau} \right\} \\ &= \arg \max_{\tilde{\tau} \in \mathcal{T}} \left\{ (\kappa + 1) \sum_{\tau \leq \tilde{\tau}} \tau \pi_{\tau} - \tilde{\tau} \mathbb{P}(\tau \leq \tilde{\tau} | Y) + \kappa \tilde{\tau} (1 - \mathbb{P}(\tau \leq \tilde{\tau} | Y)) \right\} \\ &= \arg \max_{\tilde{\tau} \in \mathcal{T}} \left\{ (\kappa + 1) \mathbb{E}[\tau | \tau \leq \tilde{\tau}, Y] + \tilde{\tau} [\kappa - (\kappa + 1) \mathbb{P}(\tau \leq \tilde{\tau} | Y)] \right\}, \end{aligned}$$

that is, $\hat{\tau} = \arg \max_{\tilde{\tau} \in \mathcal{T}} g(\tilde{\tau})$, where g is last expression within brackets above. Clearly, $g(0) = 0$; in general,

$$g(j) = (\kappa + 1) \sum_{i=0}^j i \pi_i + j [\kappa - (\kappa + 1) \sum_{i=0}^j \pi_i] = \kappa j + (\kappa + 1) \underbrace{\sum_{i=0}^j (j - i) \pi_i}_{\doteq s_j}.$$

But since $s_j = j \sum_{i=0}^j \pi_i - \sum_{i=0}^j i \pi_i$, it follows that

$$s_{j+1} = (j+1) \left(\sum_{i=0}^j \pi_i + \pi_{j+1} \right) - \sum_{i=0}^j i \pi_i - (j+1) \pi_{j+1} = s_j + \sum_{i=0}^j \pi_i.$$

Thus,

$$g(j+1) = \kappa(j+1) - (\kappa+1) \left(s_j + \sum_{i=0}^j \pi_i \right) = g(j) + \kappa - (\kappa+1) \sum_{i=0}^j \pi_i,$$

and so $g(j+1) > g(j)$ if and only if $\kappa - (\kappa+1) \sum_{i=0}^j \pi_i$, that is, $\kappa > \sum_{i=0}^j \pi_i / (1 - \sum_{i=0}^j \pi_i)$, when κ exceeds the cumulative odds. Thus, since $\sum_{i=0}^j \pi_i$ is non-decreasing, we conclude that

$$\hat{\tau} = \max \left\{ \tilde{\tau} \in \mathcal{T} : \sum_{\tau=0}^{\tilde{\tau}} \pi_{\tau} < \frac{\kappa}{1+\kappa} \right\},$$

so we propose to expand the basis expansion up to when the cumulative posterior exceeds the $\kappa/(1+\kappa)$ threshold.

A.3 ECM Specifics: Spike and Slab Variable Selection

For a particular θ_j and τ_j we have:

$$Y | \theta, \tau \stackrel{\text{ind}}{\sim} \text{Po}(\exp(D_{X_j}(v)^\top \theta))$$

and $\theta | \tau \sim N(0, \Sigma)$ where $\Sigma = \lambda^{-1} M_\tau^{1/2} (D_{X_j}^\top L_w D_{X_j})^{-1} M_\tau^{1/2}$ and $M_\tau = \text{Diag}_{i=1 \dots K} \{ \mathbf{I}(i > \tau) V_0 + \mathbf{I}(i \leq \tau) \}$. τ is as defined in (3.2). We wish to optimize the expected log joint (Dempster et al. 1977):

$$Q(\theta; \theta^{(t)}) = \mathbb{E}_{\tau | Y; \theta^{(t)}} [\log \mathbb{P}(\theta, \tau | Y)]. \quad (\text{A.1})$$

Thus, for the E-step we need,

$$\nu_i^{(t)} = \mathbb{E}[\mathbf{I}(i > \tau)] = \sum_{l=1}^{i-1} \mathbb{P}(\tau = l | Y, \theta^{(t)})$$

where

$$\mathbb{P}(\tau = l | Y, \theta^{(t)}) = \frac{\mathbb{P}(\theta^{(t)} | \tau = l) \mathbb{P}(\tau = l)}{\sum_{l=1}^K \mathbb{P}(\theta^{(t)} | \tau = l) \mathbb{P}(\tau = l)}.$$

Next we update θ by maximizing the expected log likelihood given in (A.1).

$$Q(\theta; \theta^{(t)}) = c - v \exp(D_{X_j}(v)^\top \theta^{(t)}) + \sum_v Y_v (D_{X_j}(v)^\top \theta^{(t)}) - \frac{\lambda}{2} \mathbb{E}[\theta^{(t)\top} M_\tau^{-1/2} (D_{X_j}^\top L_w D_{X_j}) M_\tau^{-1/2} \theta^{(t)}].$$

We see that updating θ is equivalent to fitting a Poisson regression with prior precision on θ . More specifically, we have

$$\mathbb{E}[\theta^{(t)\top} M_\tau^{-1/2} (D_{X_j}^\top L_w D_{X_j}) M_\tau^{-1/2} \theta^{(t)}] = \theta^{(t)\top} [T(v^{(t)}) \circ (D_{X_j}^\top L_w D_{X_j})] \theta^{(t)}$$

where \circ is the Hadamard (element-wise) product and

$$T(v) = [1 - \nu_{\max\{i,k\}} + (\nu_{\max\{i,k\}} - \nu_{\min\{i,k\}}) V_0^{-\frac{1}{2}} + \nu_{\min\{i,k\}} V_0^{-1}]_{i,k=1,\dots,K}.$$

B Model Inference

B.1 EM Specifics: Finding the MAP Coefficient Estimates

Let δ be a vector of the current parameters: ζ , ω , and θ . We have: $\mathbb{P}(Y | \delta) = \sum_z \mathbb{P}(Y, Z | \delta)$, with $Y_v | Z_v, \delta \stackrel{\text{ind}}{\sim} \text{Po}(\exp(Z_v \zeta + (1 - Z_v) D_X(v)^\top \theta))$ and $Z_v | \delta \stackrel{\text{ind}}{\sim} \text{Bern}(\text{logit}^{-1}(D_U(v)^\top \omega))$. Again, we wish to maximize the expected log joint:

$$\begin{aligned} Q(\delta; \delta^{(t)}) &= \mathbb{E}_{Z | Y; \delta^{(t)}} [\log \mathbb{P}(Y, Z | \delta)] \\ &= \underbrace{\mathbb{E}_{Z | Y; \delta^{(t)}} [\log \mathbb{P}(Y | Z, \delta)]}_{Q_1} + \underbrace{\mathbb{E}_{Z | Y; \delta^{(t)}} [\log \mathbb{P}(Z | \delta)]}_{Q_2}. \end{aligned} \tag{B.1}$$

For the E-step we need $\pi_v^{(t)} \doteq \mathbb{E}_{Z | Y; \delta^{(t)}} [Z_v]$, that is,

$$\pi_v^{(t)} = \frac{\mathbb{P}(Y_v | Z_v = 1, \theta^{(t)}) \mathbb{P}(Z_v = 1 | \omega^{(t)})}{\sum_{\tilde{Z}_v \in \{0,1\}} \mathbb{P}(Y_v | \tilde{Z}_v, \theta^{(t)}, \zeta^{(t)}) \mathbb{P}(\tilde{Z}_v | \omega^{(t)})}.$$

It follows that $\pi_v^{(t)} = \gamma_v(\omega^{(t)}, \zeta^{(t)}, \theta^{(t)})$ with γ_v as in 4.2. Next, we update ζ , θ , and ω by maximizing the expected log likelihood given in (B.1). From the first part:

$$\begin{aligned}
Q_1 &= \mathbb{E}_{Z|Y;\delta^{(t)}} \left[\sum_v -\exp(-Z_v \zeta^{(t)} + (1 - Z_v) D_X(v)^\top \theta^{(t)}) + Y_v (Z_v \zeta^{(t)} + (1 - Z_v) D_X(v)^\top \theta^{(t)}) \right] \\
&= \mathbb{E}_{Z|Y;\delta^{(t)}} \left[\sum_v Z_v (Y_v \zeta^{(t)} - \exp(\zeta^{(t)})) + (1 - Z_v) (Y_v D_X(v)^\top \theta^{(t)} - \exp(D_X(v)^\top \theta^{(t)})) \right] \\
&= \sum_v \pi_v^{(t)} (Y_v \zeta^{(t)} - \exp(\zeta^{(t)})) + (1 - \pi_v^{(t)}) (Y_v D_X(v)^\top \theta^{(t)} - \exp(D_X(v)^\top \theta^{(t)})) \\
&= \sum_v \pi_v^{(t)} Y_v (\zeta^{(t)} + \log \pi_v^{(t)}) - \pi_v^{(t)} Y_v \log \pi_v^{(t)} - \exp(\zeta^{(t)} + \log \pi_v^{(t)}) + (1 - \pi_v^{(t)}) Y_v (D_X(v)^\top \theta^{(t)} \\
&\quad + \log(1 - \pi_v^{(t)})) - (1 - \pi_v^{(t)}) Y_v \log(1 - \pi_v^{(t)}) - \exp(D_X(v)^\top \theta^{(t)} + \log(1 - \pi_v^{(t)})).
\end{aligned}$$

Analyzing the terms that contain ζ , we see that updating ζ is equivalent to fitting a quasi-Poisson regression with non-integer response, $\pi^{(t)} Y$. We have $\pi^{(t)} Y \sim \text{Quasi-Po}[\exp(\zeta + \log \pi^{(t)})]$. Similarly, we update θ where $(1 - \pi^{(t)}) Y \sim \text{Quasi-Po}[\exp(D_X \theta + \log(1 - \pi^{(t)}))]$ and we use prior precision $\lambda_\theta D_X^\top L_{w(\psi)} D_X$. Now, from the second part:

$$\begin{aligned}
Q_2 &= \mathbb{E}_{Z|Y;\delta^{(t)}} \left[Z_v \log(\text{logit}^{-1}(D_U(v)^\top \omega^{(t)})) + (1 - Z_v) \left(1 - \log(\text{logit}^{-1}(D_U(v)^\top \omega^{(t)})) \right) \right] \\
&= \sum_v \pi_v^{(t)} \log(\text{logit}^{-1}(D_U(v)^\top \omega^{(t)})) + (1 - \pi_v^{(t)}) \left(1 - \log(\text{logit}^{-1}(D_U(v)^\top \omega^{(t)})) \right).
\end{aligned}$$

Using similar reasoning as in the previous step, we update ω using a quasi-Bernoulli regression. That is, $\pi^{(t)} \sim \text{Quasi-Bern}[\text{logit}^{-1}(D_U \omega)]$. We use prior precision $\lambda_\omega D_U^\top L_{w(\psi)} D_U$.

B.2 Sampling Algorithm

Given initial estimates found from the EM algorithm presented in the preceding section, we now turn our attention to the Gibbs sampler and the conditional distributions in (4.1). Letting $\Sigma = \lambda_\theta^{-1}(D_X^\top L_{w(\psi)} D_X)^{-}$ we have for ζ and θ

$$\mathbb{P}(\zeta, \theta \mid \omega, Y_v, Z_v) \propto \prod_v \text{Po} \left[\exp \left(Z_v \zeta + (1 - Z_v)(D_X(v)^\top \theta) \right) \right] \mathbf{N}(0, \Sigma).$$

It follows, similarly to Section B.1, that up to a constant,

$$\begin{aligned} \log \mathbb{P}(\zeta, \theta \mid \omega, Y_v, Z_v) &= \sum_v -\exp \left(Z_v \zeta + (1 - Z_v) D_X(v)^\top \theta \right) + Y_v \left(Z_v \zeta + (1 - Z_v) D_X(v)^\top \theta \right) - \frac{1}{2} \theta^\top \Sigma^{-1} \theta \\ &= \sum_v Z_v \left(Y_v \zeta - \exp(\zeta) \right) + (1 - Z_v) \left(Y_v D_X(v)^\top \theta - \exp(D_X(v)^\top \theta) \right) - \frac{1}{2} \theta^\top \Sigma^{-1} \theta \end{aligned}$$

and so, isolating the terms for $Z_v = 0$ and $Z_v = 1$ containing θ and ζ respectively, we see that

$$Y_v \mid Z_v = 0 \stackrel{\text{ind}}{\sim} \text{Po}(\exp D_X(v)^\top \theta) \quad \text{and} \quad Y_v \mid Z_v = 1 \stackrel{\text{ind}}{\sim} \text{Po}(e^\zeta),$$

with prior distribution on θ described in (2.4). An analogous derivation shows that

$$Z_v \stackrel{\text{ind}}{\sim} \text{Bern}(\text{logit}^{-1} D_U(v)^\top \omega).$$

That is, sampling ζ, θ and ω is equivalent to sampling from the posterior distribution of a GLM with a multivariate normal prior on the coefficients θ and ω . Sampling is done using the Riemannian manifold Metropolis adjusted Langevin algorithm (MALA), as described in Girolami & Calderhead (2011). The proposal mechanism takes into account the natural geometry of the target density and makes transition proposals that are informed by its local structure. Specifically, the proposal density is a normal distribution, with mean based on the curvature of the space along the direction of steepest gradient and covariance given by the scaled inverse Fisher information matrix of the posterior. The process, in the general case, is as follows:

1. Set $t = 1$ and begin with $\beta = \beta^{(0)}$;
2. Sample β^* from proposal density, q ;
3. Accept with probability, $\rho(\beta^{(t-1)}, \beta^*)$. If accept, $\beta^{(t)} = \beta^*$; if reject, $\beta^{(t)} = \beta^{(t-1)}$;
4. Set $t = t + 1$ and return to step 2;

where

$$\rho(\beta^{(t-1)}, \beta^*) = \min\left(1, \frac{\pi(\beta^*)q(\beta^*, \beta^{(t-1)})}{\pi(\beta^{(t-1)})q(\beta^{(t-1)}, \beta^*)}\right).$$

Here $q(\beta^*|\beta^n, \epsilon) = N(\beta^*|\mu(\beta^n, \epsilon), \epsilon^2 G^{-1}(\beta^n))$ where

$$\begin{aligned} \mu(\beta^n, \epsilon)_i &= \beta_i^n + \frac{\epsilon^2}{2} \{G^{-1}(\beta^n) \nabla_{\beta} \log\{p(\beta^n)\}\}_i - \epsilon^2 \sum_{j=1}^D \{G^{-1}(\beta^n) \frac{\partial G(\beta^n)}{\partial \beta_j} G^{-1}(\beta^n)\}_{ij} + \\ &\quad \frac{\epsilon^2}{2} \sum_{j=1}^D \{G^{-1}(\beta^n)\}_{ij} \text{tr} \left\{ G^{-1}(\beta^n) \frac{\partial G(\beta^n)}{\partial \beta_j} \right\}, \end{aligned}$$

ϵ is a step parameter, and G is the Fisher information matrix of the posterior distribution. That is, with Σ defined as above, $G(\beta) = \mathbb{E}[-\frac{\partial^2 \mathbb{P}(\beta|y)}{\partial \beta \partial \beta^\top}] = X^\top \Omega(\beta) X + \Sigma^{-1}$ and $\frac{\partial G}{\partial \beta_i} = X^\top \Omega(\beta) V^i X$. In the logistic model, given the logit link function:

- $\Omega(\omega)_{v,v} = \text{logit}^{-1}(D_U(v)^\top \omega) (1 - \text{logit}^{-1}(D_U(v)^\top \omega))$
- $V^i = (1 - 2\text{logit}^{-1}(D_U(v)^\top \omega)) D_U(v)_i$

in accordance with the example in Section 7 of (Girolami & Calderhead 2011). For the Poisson model, with the log link function, we have:

- $\Omega(\theta)_{v,v} = \exp(D_X(v)^\top \theta)$
- $V^i = D_X(v)_i$.

We use a step size based on the recommendation of Roberts & Rosenthal (1998) on the order of $D^{-1/3}$ where D is the dimension of the parameter space. In practice, this resulted in an acceptance rate of approximately 75%.

B.3 Posterior distribution of linear predictors based on Gibbs Sampling

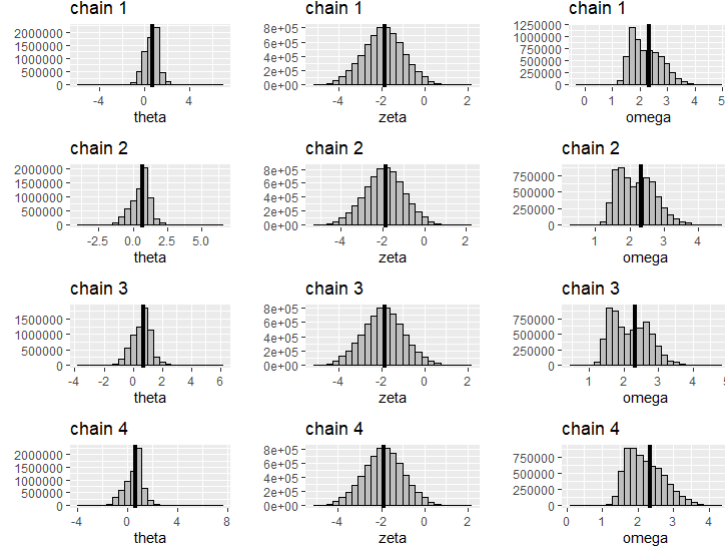


Figure 10: The linear predictors (i.e. $D_X\theta$, $X\zeta$, and $D_U\omega$). Per the sampling scheme, there are 1000 values for each residential intersection in Boston.

Here we plot the posterior distributions of the linear predictors and superimpose the results from the EM algorithm point estimates; they are in agreement. The analysis was run on a MacBook Pro laptop, with an Apple M2 chip featuring 8 cores, comprising 4 performance and 4 efficiency cores. The system is outfitted with 16 GB of memory and no parallelization scheme was implemented. As a point of comparison, the EM algorithm ran quite quickly (~ 21 minutes), but running the entire Gibbs sampling scheme as described in the paper (4 chains) took ~ 4 days. We leave the choice to the practitioner. The network is composed of 12,763 nodes (i.e. street segments).

C Boston Neighborhoods

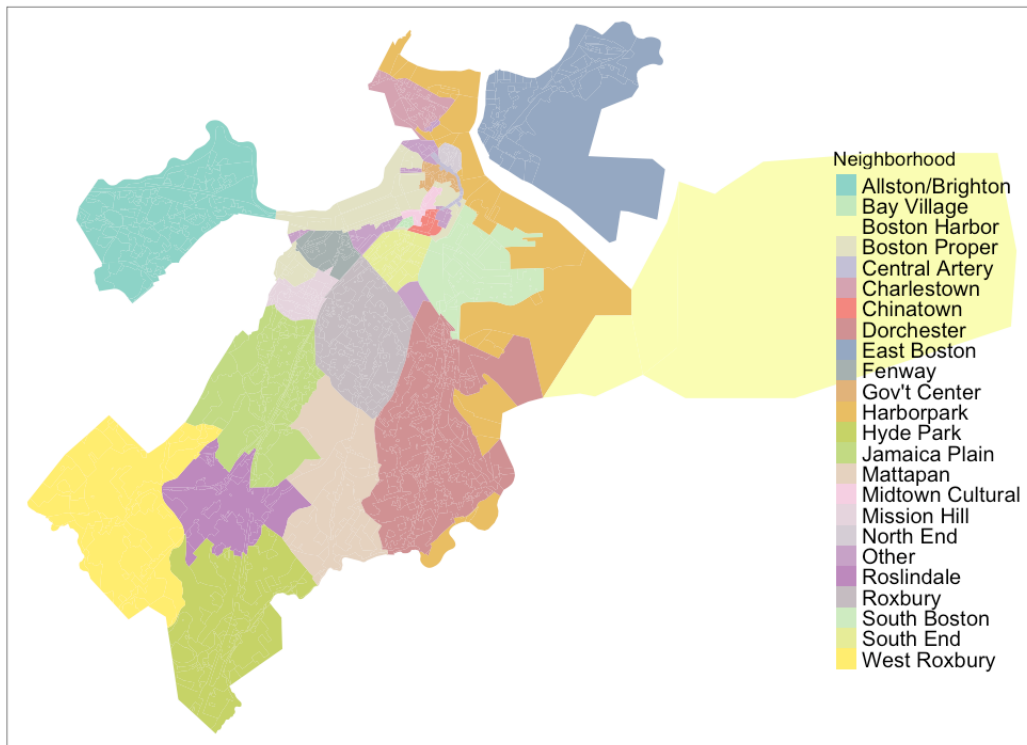


Figure 11: Neighborhood designations in Boston, MA.

References

- Balocchi, C. & Jensen, S. T. (2019), ‘Spatial modeling of trends in crime over time in philadelphia’, *The Annals of Applied Statistics* **13**(4), 2235–2259.
- Banerjee, S., Carlin, B. P. & Gelfand, A. E. (2014), *Hierarchical Modeling and Analysis for Spatial Data*, CRC Press.
- Belkin, M., Matveeva, I. & Niyogi, P. (2004), Regularization and semi-supervised learning on large graphs, *in* ‘International Conference on Computational Learning Theory’, Springer, pp. 624–638.
- Bernasco, W. & Block, R. (2009), ‘Where offenders choose to attack: A discrete choice model of robberies in Chicago’, *Criminology* **47**(1), 93–130.

- Besag, J., York, J. & Mollié, A. (1991), ‘Bayesian image restoration, with two applications in spatial statistics’, *Annals of the institute of statistical mathematics* **43**, 1–20.
- Bowers, K. J., Johnson, S. D. & Pease, K. (2004), ‘Prospective hot-spotting: the future of crime mapping?’, *British journal of criminology* **44**(5), 641–658.
- City of Boston (2016), ‘Data Boston’, <https://data.cityofboston.gov/>. Retrieved February 16, 2016.
- City of Boston (2022), ‘Boston Housing Conditions and Real Estate Trends Report’, <https://www.bostonplans.org/getattachment/066b23c5-cab9-4731-a338-f6e57e3ef55f>. Retrieved January 8, 2023.
- Cleveland, C., Stanton, L., Woods, B., Martin, A., Fortune, D., Walsh, M., Castigliego, J., Perez, T., Galante, E. et al. (2019), ‘Carbon free boston: Social equity report 2019’.
- Cormen, T. H., Leiserson, C. E., Rivest, R. L. & Stein, C. (2001), *Introduction to Algorithms*, Vol. 6, MIT press Cambridge.
- Davies, T. & Johnson, S. D. (2015), ‘Examining the relationship between road structure and burglary risk via quantitative network analysis’, *Journal of Quantitative Criminology* **31**, 481–507.
- Dempster, A. P., Laird, N. M. & Rubin, D. B. (1977), ‘Maximum likelihood from incomplete data via the EM algorithm’, *Journal of the Royal Statistical Society Series B* **39**(1), 1–38.
- Dorfler, F. & Bullo, F. (2012), ‘Kron reduction of graphs with applications to electrical networks’, *IEEE Transactions on Circuits and Systems I: Regular Papers* **60**(1), 150–163.
- Eck, J., Chainey, S., Cameron, J. & Wilson, R. (2005), Mapping crime: Understanding hotspots, Technical report, National Institute of Justice.
- Frith, M. J., Johnson, S. D. & Fry, H. M. (2017), ‘Role of the street network in burglars’ spatial decision-making’, *Criminology* **55**(2), 344–376.
- Garner, B. A. (2001), *A Dictionary of Modern Legal Usage*, Oxford University Press, USA.
- George, E. I. & McCulloch, R. E. (1993), ‘Variable selection via gibbs sampling’, *Journal of the American Statistical Association* **88**(423), 881–889.

- Girolami, M. & Calderhead, B. (2011), ‘Riemann manifold langevin and hamiltonian monte carlo methods’, *Journal of the Royal Statistical Society: Series B (Statistical Methodology)* **73**(2), 123–214.
- Johnson, S. D., Guerette, R. T. & Bowers, K. (2014), ‘Crime displacement: what we know, what we don’t know, and what it means for crime reduction’, *Journal of Experimental Criminology* **10**, 549–571.
- Kim, S., Joshi, P., Kalsi, P. S. & Taheri, P. (2018), Crime analysis through machine learning, in ‘2018 IEEE 9th Annual Information Technology, Electronics and Mobile Communication Conference (IEMCON)’, IEEE, pp. 415–420.
- Kolaczyk, E. D. (2009), *Statistical Analysis of Network Data*, Springer.
- Kolaczyk, E. D. & Csárdi, G. (2014), *Statistical Analysis of Network Data with R*, Springer.
- Lanckriet, G. R., De Bie, T., Cristianini, N., Jordan, M. I. & Noble, W. S. (2004), ‘A statistical framework for genomic data fusion’, *Bioinformatics* **20**(16), 2626–2635.
- Leskovec, J. & Krevl, A. (2014), ‘SNAP Datasets: Stanford Large Network Dataset Collection’, <http://snap.stanford.edu/data>. Retrieved March 23, 2017.
- Li, C. & Li, H. (2008), ‘Network-constrained regularization and variable selection for analysis of genomic data’, *Bioinformatics* **24**(9), 1175–1182.
- Li, T., Levina, E. & Zhu, J. (2019), ‘Prediction models for network-linked data’, *The Annals of Applied Statistics* **13**(1), 132–164.
- Mahfoud, M., Bhulai, S., van der Mei, R., Erkin, D. & Dugundji, E. (2019), ‘Network analysis of city streets: forecasting burglary risk in small areas’, *International Journal On Advances in Security*.
- McCullagh, P. & Nelder, J. A. (1989), *Generalized Linear Models*, Chapman & Hall.
- Meijer, A. & Wessels, M. (2019), ‘Predictive policing: Review of benefits and drawbacks’, *International Journal of Public Administration* **42**(12), 1031–1039.

- Meng, X.-L. & Rubin, D. B. (1993), ‘Maximum likelihood estimation via the ECM algorithm: A general framework’, *Biometrika* **80**(2), 267–278.
- Mohler, G. O., Short, M. B., Brantingham, P. J., Schoenberg, F. P. & Tita, G. E. (2011), ‘Self-exciting point process modeling of crime’, *Journal of the American Statistical Association* **106**(493), 100–108.
- Open Data (2016), ‘Boston Maps’, <http://bostonopendata-boston.opendata.arcgis.com/>. Retrieved February 16, 2016.
- Palmer, C. J., Pathak, P. A. et al. (2017), Gentrification and the amenity value of crime reductions: Evidence from rent deregulation, Technical report, National Bureau of Economic Research.
- Porta, S., Crucitti, P. & Latora, V. (2006), ‘The network analysis of urban streets: A dual approach’, *Physica A: Statistical Mechanics and its Applications* **369**(2), 853–866.
- Ramsay, J. & Silverman, B. W. (2005), *Functional Data Analysis*, Springer.
- Robert, C. & Casella, G. (2013), *Monte Carlo statistical methods*, Springer Science & Business Media.
- Roberts, G. O. & Rosenthal, J. S. (1998), ‘Optimal scaling of discrete approximations to langevin diffusions’, *Journal of the Royal Statistical Society: Series B (Statistical Methodology)* **60**(1), 255–268.
- Ročková, V. & George, E. I. (2014), ‘Emvs: The em approach to bayesian variable selection’, *Journal of the American Statistical Association* **109**(506), 828–846.
- Smola, A. J. & Kondor, R. (2003), Kernels and regularization on graphs, in ‘Learning Theory and Kernel Machines’, Springer, pp. 144–158.
- Vehtari, A., Gelman, A., Simpson, D., Carpenter, B. & Bürkner, P.-C. (2019), ‘Rank-normalization, folding, and localization: An improved r-hat for assessing convergence of mcmc’, *arXiv preprint arXiv:1903.08008*.